Improving Air Quality Model Predictions of Organic Species using Measurement-Derived Organic Gaseous and Particle Emissions in a Petrochemical-Dominated Region

Craig A Stroud[1], Paul A Makar[1], Junhua Zhang[1], Michael D. Moran[1], Ayodeji Akingunola[1], Shao-Meng Li[1], Amy Leithead[1], Katherine Hayden[1], and May Siu[2]

[1]Air Quality Research Division, Environment and Climate Change Canada, 4905 Dufferin Street, Toronto, Ontario, M3H 5T4, Canada
[2]Air Quality Research Division, Environment and Climate Change Canada, 335 River Road, Ottawa, Ontario, K1V 1C7, Canada

Corresponding author: Craig A. Stroud (craig.stroud@canada.ca)

Abstract

This study assesses the impact of revised volatile organic compound (VOC) and organic aerosol (OA) emissions estimates in the GEM-MACH (Global Environmental Multiscale–Modelling Air Quality and CHemistry) chemical transport model on air quality model predictions of organic species for the Athabasca oil sands region in Northern Alberta, Canada. The first emissions dataset that was evaluated (base-case run) makes use of regulatory-reported VOC and particulate matter emissions data for the large oil sands mining facilities. The second emissions dataset (sensitivity run) uses total facility emissions and speciation profiles derived from box-flight aircraft observations around specific facilities. Large increases in some VOC and OA emissions in the revised-emissions data set for four large oil sands mining facilities and decreases for others were found to improve the modeled VOC and OA concentration maxima in facility plumes, as shown with the 99th percentile statistic and illustrated by case studies. The results show that the VOC emission speciation profile from each oil sand facility is unique and different from standard petrochemical-refinery emission speciation profiles used for other regions in North America. A significant increase in the correlation coefficient is reported for the long-chain alkane predictions against observations when using the revised emissions based on

aircraft observations. For some facilities, larger long chain alkane emissions resulted in higher secondary organic aerosol production, which improved OA predictions in those plumes. Overall, the use of the revised emissions data resulted in an improvement of the model mean OA bias; however, a decrease in OA correlation coefficient and a remaining negative bias suggests the need for further improvements to model OA emissions and formation processes. The weight of evidence suggests that the top-down emission estimation technique helps to better constrain the fugitive organic emissions in the oil sands region, which are a challenge to estimate given the size and complexity of the oil sands operations and the number of steps in the process chain from bitumen extraction to refined oil product. This work shows that top-down emissions estimation technique may help to constrain bottom-up emission inventories in other industrial regions of the world with large sources of VOCs and OA**.**

1 Introduction

Chemical transport models (CTMs) are useful tools to support clean energy policy decisions because they can be used to assess the impact of past and future pollutant emission changes on air quality (e.g., Schultz *et al*., 2003; Kelly *et al*., 2012; Rouleau *et al*., 2013; Lelieveld *et al.*, 2015). CTMs can also be run in forecast mode with their output being used to support air quality forecasts (Moran *et al.*, 2010; Chai *et al*., 2013). CTMs require pollutant emission inputs, typically at hourly intervals, at the model grid spatial resolution (Dickson and Oliver, 1991; Houyoux *et al*., 2003; Pouliot *et al*., 2012, 2015; Zhang *et al*., 2017). The pollutant emission input files are based on the processing of emission inventories compiled for all emission sectors, usually at some geopolitical spatial resolution (e.g., county, province/state, or country), and may thus require the application of spatial disaggregation factor fields to allocate emissions to the model grid. North American emission inventories are typically derived from bottom-up

approaches, where representative pollutant emission factors (e.g., pollutant mass emission per volume of fuel burned) are multiplied by activity factors (e.g., volume of fuel burned per unit time). In developed countries, industrial facilities are usually required to report estimates of their pollutant emissions to national inventories such as the National Pollutant Release Inventory (NPRI) in Canada (Government of Canada, Canada Gazette, 2018) and the National Emissions Inventory (NEI) in the United States (Office of the Federal Register, Protection of Environment, 2015). Updates of these inventories occur under a regulatory framework on a regular basis. However, reporting requirements may be limited to aggregated mass emissions on an annual basis (e.g., a total bulk mass of VOC emitted rather than a detailed and observation-based emissions of individual speciated VOCs), with the subsequent use of VOC speciation profiles (splitting factors) to determine the relative contribution of the individual VOCs to the total VOC emissions. Uncertainties in the availability and assignment of appropriate VOC speciation profiles, spatial and temporal allocation factors (Mashayekhi *et al*., 2016), and/or unaccounted-for emitting activities, result in the need to evaluate the impact of these assumptions through the comparison of CTM predictions with ambient observations.

The Athabasca region of northeastern Alberta, Canada has one of the largest reserves of oil sands (OS) in the world. The OS deposits are composed of bitumen, minerals, sand and clay. Oil sand near the surface is mined by open-pit mining techniques. The oil sand is then transported by heavy hauler trucks to crushers, followed by the addition of hot water to make the oil sand flow through pipelines to a bitumen extraction facility. Here, the bitumen is separated from the sand and clay by the use of organic solvents. The product is used either directly, upgraded on-site to crude oil or transported to a remote upgrader facility. Volatile organic compounds from the bitumen have the potential to escape into the atmosphere as fugitive emissions during the

mining, extraction, processing, or tailing discharge steps. The complexity and vast size of the oil sands operations make generating pollutant emission input files for CTMs a challenge (Cho *et al*., 2012; ECCC & AEP, 2016).

Organic compounds in the atmosphere are oxidized over time and, in the presence of sufficient levels of oxides of nitrogen, are important precursors to ozone formation (Seinfeld and Pandis, 1998). VOCs and semi-volatile organic compounds (SVOCs) are also precursors to secondary organic aerosol (SOA) formation (Griffin *et al*., 1999; Kanakidou *et al*., 2005; Robinson *et al*., 2007; Kroll and Seinfeld, 2008; Slowik *et al*., 2010; Stroud *et al*., 2011; Gentner *et al*., 2017). If the organic compounds have sufficiently low saturation vapor pressures, then upon release into the atmosphere they remain particle-bound and are classified as primary organic aerosol (POA). Many specific organic compounds can also be toxic to human health and require explicit reporting in emission inventories (Stroud *et al*., 2016).

The Joint Oil Sands Monitoring (JOSM) program was developed by the federal government of Canada and the Alberta provincial government with input and consultation from the local indigenous population and industry stakeholder groups to monitor the potential impacts of pollutant emissions. During JOSM, top-down approaches to estimate emissions based on atmospheric observations provided a unique opportunity to compare with bottom-up calculated emissions for the Athabasca OS facilities in Alberta, Canada (Gordon *et al*, 2015; Li *et al*., 2017). The mass-balance approach that was used is based on using box-shaped aircraft flight patterns around a facility and measuring pollutant concentrations and meteorological variables (wind speed and direction, air density). In this approach, the difference in pollutant mass fluxes entering and leaving the box is used to determine the total facility-wide emission rate, subject to

assumptions such as minimal losses due to chemical oxidation between the emissions location and the nearby aircraft observations.

Environment and Climate Change Canada (ECCC)'s chemical transport model, GEM-MACH (Global Environmental Multi-scale-Modelling Air quality and CHemistry) is being used in JOSM to assess the impact of current emissions and future emission changes on local air quality and downwind regional-scale acid deposition (Makar *et al.*, 2018). In this model study, we make use of both regulatory-inventory-based and aircraft-observation-derived emissions data for VOCs and primary particulate emissions for six large OS mining facilities as inputs to GEM-MACH in order to assess the impact of these two different emission data sets on model predictions of VOC concentrations and organic aerosol (OA) formation.

2 Methods

The GEM-MACH model uses the ECCC operational weather forecast model (GEM) as the core operator for dynamics and microphysical processes (Côté *et al*., 1998a,b; Girard *et al*., 2014). GEM-MACH is an "on-line" CTM - the chemistry, vertical diffusion, and pollutant deposition routines exist as a set of subroutines contained and called from within GEM's meteorological physics package (Moran *et al.*, 2010, Makar *et al*., 2015ab). The gas-phase chemistry scheme is based on the ADOM-II mechanism, originally developed for continental boundary-layer oxidant formation. The VOC lumped species used in GEM-MACH are described in Stroud *et al*. (2008). The focus here is on evaluating volatile aromatic and alkane species of anthropogenic origin. The aerosol size distribution is described by a 12-bin sectional approach based on the Canadian Aerosol Module (CAM) (Gong *et al*., 2003; Park *et al*., 2011). The SOA scheme is based on a two-product fit to smog chamber data using the SOA yield equations derived from gas/particle partitioning theory (Pankow 1994; Griffin *et al*., 1999; Barsanti et al.,

2013). In the GEM-MACH model's current SOA formation algorithms, after initial particle formation, the organic compounds in the particle phase are assumed to be converted rapidly to non-volatile mass, as observed by recent studies (Cappa and Jimenez, 2010; Cappa *et al*., 2011; Lopez-Hilfiker *et al*., 2016) and recommended by modelling studies (Shrivastava *et al*., 2015). However, other recent observation studies suggest that SOA 'chemical aging' over hours to days is quite complex, and involves further gas-phase oxidation and fragmentation reactions (Jimenez *et al*., 2009; Donahue *et al*., 2014), as well as potential particle-phase oxidation and oligomer reactions (McNeill *et al*., 2015). The particle oligomer reactions are rapid, often acid-catalyzed, and can result in conversion to non-volatile mass (Liggio *et al*., 2005; Kroll *et al*., 2005). We discuss below the evidence from this work on the likelihood that these additional missing processes are still impacting our model organic aerosol bias.

2.1 Emissions

The Canadian base-case emissions were derived by combining several emission inventories, targeting 2013 as the base year. This base year was chosen to align with the JOSM 2013 intensive field study period, which provided the observations for the model/observation comparisons that follow. Canadian emissions for industrial facilities, including the Athabasca OS mining facilities, were obtained from the 2013 NPRI. The U.S. base-case emissions were obtained from the 2011 U.S. NEI Version 1 (Eyth *et al*., 2013).

These base-case, bottom-up emissions inventories were processed with the SMOKE emissions processing tool (https://www.cmascenter.org/smoke), which includes three major steps corresponding to spatial allocation, temporal allocation, and chemical speciation (for NOx, VOC, and PM). The base-case VOC speciation profiles used by SMOKE for the OS surface mining

148 facilities were obtained from the CEMA (Cumulative Environmental Management Association)
149 inventory (Davies *et al*., 2012; Zhang *et al*., 2015).

150 For the sensitivity run, speciated VOC emissions from the base case for four OS mining
151 facilities (Suncor Millenium/Steepbank, Syncrude Mildred Lake, Shell Canada
152 Muskeg/Jackpine, and CNRL Horizon) were revised by replacing them with the top-down
153 emission rates estimated by Li *et al*. (2017) while primary PM emissions were revised for six oil
154 sand facilities (Suncor Millenium/Steepbank, Syncrude Mildred Lake, Shell Canada
155 Muskeg/Jackpine, CNRL Horizon, Syncrude Aurora North, and Imperial Oil Kearl) (Zhang *et*
156 *al.*, 2018). The VOC and PM chemical speciation profiles used for these facilities were also
157 revised using the aircraft-observed VOC speciation (Li *et al*., 2017) and ground-based PM filter
158 analysis (Wang *et al*., 2015), respectively. The set of emissions input files making use of these
159 revisions is hereafter referred to as the "revised emissions", while the original emissions input
160 files without these changes is referred to as the "base-case emissions". A detailed description of
161 the development of the emission inventory and emissions processing steps to create the model-
162 ready files (hourly gridded emission fields for the same domain and grid spacing as the model)
163 for the base case and revised version are described in Zhang *et al*. (2018). Table 1 compares the
164 facility emission rates for four species for the base case and revised-emissions case. The changes
165 are not consistent from species to species and are not uniform across facilities. Interestingly, the
166 facilities that use paraffinic solvents for bitumen extraction (e.g. Shell Muskeg/Jackpine) were
167 associated with the largest ALKA emission increases and aromatic decreases. The SI section
168 includes figures illustrating the emission difference maps for the oil sand region (absolute and
169 relative difference) showing the spatial distribution of emission changes between revised and
170 base case. The changes are largest over the surface mines and tailing ponds.

Depending on whether bitumen extracted from the oil sand is upgraded on site or not, the OS mining facilities can be classified into two broad types: (1) integrated extraction and upgrading facilities (Suncor Millenium/Steepbank, Syncrude Mildred Lake, and CNRL Horizon) and (2) extraction-only facilities (Shell Canada Muskeg/Jackpine, Syncrude Aurora North, and Imperial Oil Kearl). Table 2 shows a comparison of the CEMA plant-specific VOC speciation profiles used in the base case for the two types of OS plants compared to two standard VOC speciation profiles for petrochemical facilities (#9012 "Petroleum Industry – Average", #0316 "Fugitive Emissions, Pipe/Valve Flanges") that were used by SMOKE to speciate more than half of the refinery emissions in the Houston area, the largest petrochemical cluster in the U.S. There are significant differences between the base case OS plant VOC speciation profiles and the two commonly used standard oil refinery profiles. The OS integrated extraction and upgrading plant profiles are higher in long-chain alkenes, toluene, and other aromatics than the standard profiles, while the extraction-only plant profile has the highest long-chain alkane fraction. The two standard profiles used for the base case and revised simulation (for speciating U.S. and Canadian refinery emissions) have higher less-reactive species (e.g., propane, acetylene) and formaldehyde (profile #9012), than both the CEMA OS plant profiles. Note also that these differences in relative fractions result in substantial differences in the absolute emissions of certain groups of VOCs between the standard profiles for oil refineries and the facility-specific oil sand profiles. For reference, the aircraft-measurement-derived facility-specific VOC speciation profiles used for four OS facilities in the revised-emissions case are presented in Zhang *et al.* (2018). The aircraft-measurement-derived profiles in Zhang *et al.* (2018), and used here for the revised case, are composite profiles since they encompass plant, tailing pond and mining emissions. As such,

193 they are not appropriate for comparison with the profiles in Table 2, which are specific to plant
194 emissions.
195 The primary PM emissions from the OS facilities originate largely from off-road heavy-duty
196 diesel trucks, plant stack emissions, and fugitive and wind-blown dust. The 2009/10 CEMA
197 inventory was used to specify the tail-pipe emissions from the off-road mining fleet and the 2013
198 NPRI inventory was used for fugitive road-dust emissions. The base-case inventory did not
199 include wind-blown dust. For the revised inventory, the PM size distribution was measured
200 during the 2013 field study for all six facilities and these data were used to constrain the revised
201 PM emission input data set. Note that the PM emissions estimates based on the aircraft-measured
202 aerosol data included the contribution of wind-blown dust emissions. The aircraft-based PM
203 emissions were re-binned for the 12 GEM-MACH PM size bins. The first eight size bins
204 correspond to mass up to diameter 2.56 μm. Interestingly, the aircraft measured a much higher
205 fraction of particulate mass in bin 8 (bounded by diameters 1.28 and 2.56 μm) compared to the
206 mass fraction in bin 8 from the area-source PM size-distribution profiles used by SMOKE in
207 processing the base-case emissions. In addition, a PM chemical speciation profile specific to OS
208 fugitive dust emissions was created from an analysis of deposited dust collected from surfaces in
209 the OS region (Wang *et al*., 2015); this speciation profile replaced the standard fugitive dust
210 profile for unpaved roads from the U.S. EPA SPECIATE v4.3 database in the revised emissions
211 processing. The resulting organic carbon fraction in the observation-derived PM speciation
212 profile was higher than that of the base-case emissions by about a factor of 3 (Zhang *et al.*,
213 2018). In general, significantly higher POA emissions were observed over the open-pit mines for
214 all facilities, except for the Imperial Kearl mine. The impact of the revised POA emissions will
215 be discussed further in Section 3.4.

2.2 Modeling

The GEM-MACH model was run in a nested configuration with an outer domain covering the continental U.S. and Canada and an inner domain covering Alberta and Saskatchewan. The continental-scale GEM-MACH model (10-km resolution) and the Canada-wide GEM weather model (2.5-km resolution) were run first. These provided the chemical and meteorological lateral boundary conditions, respectively, for the high-resolution GEM-MACH 2.5-km resolution run, which has a domain covering the provinces of Alberta and Saskatchewan (Figure 1). The two models providing boundary conditions were run on a 30-hour cycle, of which the first six hours were spin-up and discarded, while the remaining 24 hours provided boundary conditions for the 2.5-km GEM-MACH simulation. The initial conditions subsequent to the starting model simulation for each overlapping 24-hour 2.5-km GEM-MACH simulation came from the end of the previous 2.5-km GEM-MACH simulation. This strategy was used to allow the two boundary condition simulations to make use of assimilated meteorological analyses. The sequence of model simulations was started for August 10, 2013 and run until September 7 to cover the 2013 JOSM intensive field study period.

2.3 Observations

The NRC (National Research Council) Convair two-engine turboprop aircraft was used to collect air-quality observations during the JOSM 2013 intensive field study. The aircraft was equipped with a suite of instruments to measure air quality over 22 flights (see Li *et al.*, 2017, Figure S1). Most of the flight hours focused on “box” flight paths; these took the aircraft around the periphery of facilities at different heights, with the goal of deriving facility-wide emission rates by using observations of chemical concentrations and winds to estimate the mass of pollutants entering and leaving the box enclosures. Coupled with a mass-conserving flux model

(Gordon *et al*., 2015), these aircraft data were used to estimate emissions from the encircled facilities.

VOC and PM observations were collected by the instrumented research aircraft using different technologies. A proton-transfer-reaction mass spectrometer (PTR-MS) was used to measure a select number of VOCs at high temporal resolution (1-sec) (Li *et al*., 2017). An aerosol mass spectrometer (AMS) was used to measure PM_1 mass and non-refractory chemical composition (Liggio *et al*., 2016). A Single Particle Soot Photometer (SP2) was used to measure refractory black carbon aerosol (Liggio *et al*., 2016). A number of canisters were filled with ambient air on each flight and returned to the lab for GC-FID and GC-MS analysis of VOCs (Li *et al*., 2017). The canister VOC analysis measured 154 different C_2 to C_{12} hydrocarbons (Dann and Wang, 1995). The resulting observation data were compared to the model output generated as described above. The 2.5-km GEM-MACH runs used a 120-s chemistry time step; 120-s model output values were linearly interpolated in time and space to the aircraft observation locations; all comparisons which follow make use of the resulting model/observation data pairs for the two simulations.

3 Results and Discussion

We present our evaluation results for four species classes: mono-substituted aromatics in section 3.1; multi-substituted aromatics in section 3.2; long-chain alkane species in section 3.3; and organic aerosols in section 3.4.

3.1 Toluene and other Mono-Substituted Aromatics (TOLU) Evaluation

The aircraft PTR-MS measurement data set was averaged to 10-sec intervals for comparison to the GEM-MACH model output. The model grid cell output was extracted along the flight track and interpolated linearly between the two minute model output intervals to create a

coincident model and measurement time series. The model lumped TOLU species includes toluene and other mono-substituted aromatics with the two most important additional species being ethyl-benzene and propyl-benzene. Therefore, we must derive an equivalent observed lumped TOLU species for a comparison. We used all of the canister VOC data from the field study to create ethyl-benzene vs. toluene and propyl-benzene vs. toluene scatterplots. The corresponding slope, y-intercept and correlation coefficient for both these plots (not shown) were as follows: m=0.376±0.006, y=0.0328±0.006, R=0.91 and m=0.0652±0.0008, y-intercept=0.0011±0.0008, R=0.90, respectively. Thus, we derived an observed TOLU equal to the PTR-MS C7 aromatic multiplied by the factor 1.4412 (sum of m=1.0 C7+0.376 C7+0.0652 C7). This new observation-derived TOLU was used in the statistical comparison with model output TOLU, which follows.

Histograms of mixing ratio were created using the observed TOLU, the revised-emissions model output, and the base-case model output. Figure 2 illustrates the histograms using 20 mixing-ratio bins and an increment of 0.2 ppbv per bin. It is clear that there are more high values (>2 ppbv) produced by the sensitivity model run with revised emissions compared to the base-case model run. The number of observations in the highest value bins lies between the results from the revised and base-case versions. This can be quantified by using the 99% percentile statistic (obs=1.258 ppbv, revised=1.906 ppbv, base=0.934 ppbv). The 99% percentile means that 99% of the data points are lower than the value. The median concentration of the observations (0.061 ppbv) is higher than both the revised (0.038 ppbv) and base-case model (0.019 ppbv) simulated values, but is closer to the revised version. Table 3 lists statistical scores for the TOLU lumped species and the other species considered in this study. The mean bias goes from a negative value with the base-case run to a positive value with the revised emissions.

There is little difference in the correlation coefficient for the model vs. observation scatterplot between the base-case and sensitivity run. The changes to the VOC emissions for the revised-emissions run affected their total mass and speciation, and the observations were made sufficiently close to the sources that there was little time for oxidation. The main sources for VOCs are the processing plants, tailing ponds, mine faces, and off-road vehicles and their spatial allocation (from CEMA, 2010) did not change significantly between the two model-emission versions. The main differences in the model time series between the two simulations are thus in magnitude of concentrations, and hence relatively invariant correlation coefficients might be expected. The correlation coefficient is more likely controlled by the meteorological model accuracy in the placement of the plumes (i.e. wind direction).

The largest increases in the TOLU emission, between the revised and base case run, are noted for the Syncrude Mildred Lake facility over the tailing ponds and open pit mine faces. Table 1 shows the changes on a facility-wide level. Notable increases are also calculated for the Suncor Millennium/Steepbank and the Canadian Natural Resources Ltd (CNRL) Horizon facilities. The flights on August 14 and 23 have the largest TOLU mixing ratios for the aircraft study, and both flights correspond to box flights around the Syncrude Mildred Lake facility. The SI section includes the model and measurement time series comparisons (termed case studies) for the flights on August 14 (Figure S5) and August 23 (Figure S6). Overall, the magnitude of the mixing ratio maximum in the time series are better represented in the revised-emission simulation. This is also reflected in the better slope statistic in Table 3 for the revised-emission simulation.

3.2 Multi-Substituted Aromatics (AROM) Evaluation

The model lumped AROM species includes all multi-substituted aromatics, with the most important species being the xylene isomers and trimethylbenzene isomers. These two species match with the PTR-MS C8 and C9 aromatic fragments, respectively. However, the observed C8 aromatic also includes ethyl-benzene and the C9 aromatic also includes propyl-benzene, which are lumped with TOLU in the model VOC speciation. Thus, we need to subtract these unwanted species from the totals used to compare to the model lumped AROM species. To do this, we use their correlation slopes with PTR-MS C7 aromatic from Section 3.1. The new observation-derived AROM was calculated from the PTR-MS measurements as follows: C8 + C9 – 0.376 C7 – 0.0652 C7.

Figure 3 shows the histograms for the lumped AROM species for 10-sec averaged points along all the flight tracks. The base model has a large number of high value points (> 2ppbv), many more than the model simulations with the revised emissions, and also more than the observations. This can be quantified by using the 99% percentile (obs=0.7607, revised=1.004, base case=2.302). The median value for the observations is 0.0182 ppbv, smaller than both the model versions (revised=0.0236 ppbv, base case=0.0466 ppbv), but closer to the model driven by the revised emissions. Table 3 lists other statistical scores for the AROM lumped species. The mean bias and RMSE are smaller for the revised emissions run compared to the base case. However, there is a small degradation in the correlation coefficient with the sensitivity run.

The largest decreases in the AROM emission field between the revised and base case emissions are again over the Syncrude Mildred Lake facility (refer to Table 1). There were also notable decreases over the CNRL Horizon and Shell Muskeg/Jackpine facilities, but positive changes in AROM emissions were noted over the Suncor Millennium/Steepbank facility (also refer to Figure S2 for the emission spatial difference map). The SI section includes the model

and measurement time series comparison for the flights on August 23 and September 3. In general, the observed mixing ratio changes are closer in magnitude to the predictions from the revised-emission simulation compared to the base case for the plume intersects.

3.3 Long-Chain Alkanes (ALKA) Evaluation

The long-chain alkanes (C_4 to C_{12}) were sampled by filling canisters with ambient air on-board the aircraft. Figure 4 presents the histogram for the long-chain alkanes. The mixing ratios are divided into 20 bins each with a width of 3 ppbv. From the observed histogram, there is a wide range to the mixing ratios with a small number of very large concentrations, but also the first bin (0 to 3 ppbv) has a high percentage of the points. The model gas-phase mechanism represents all higher carbon-number alkanes by a single lumped species, with chemical and physical properties derived from C_4 to C_8 alkanes. The base-case run calculates lower ALKA mixing ratios than the model version using revised emissions. The model using revised emissions is much better at reproducing the higher concentration points, particularly above 12 ppbv. This is quantified by the 99% percentile of the data sets (obs=29.9, base=18.0 revised=24.6). Other statistics for the lumped ALKA species are shown in Table 3. The mean bias went from a small negative value to +1.98 ppbv. The slope decreased by a small value, but the y-intercept increased, which also increased the RMSE for the run with the revised emissions. The correlation coefficient improved significantly for the model run with revised emissions.

The revised ALKA emissions are considerably higher for the CNRL Horizon and Shell Muskeg/Jackpine facilities, but have smaller changes for the other facilities (refer to Table 1), possibly reflecting differences in the processing activities between the facilities. Overall, the time series analysis for the aircraft flights (refer to Figures S10 and related discussion in SI) showed mixed improvements for ALKA associated with the revised emissions. The large increases in

ALKA emissions in the sensitivity simulation for the CNRL facility did improve the model maxima for the plume intersects on August 26. The analysis suggests further improvement in spatial allocation for the Shell facility may be needed. The higher ALKA mixing ratios also feeds back to higher SOA formation downwind of these facilities, as discussed below.

The use of aircraft observations to both derive emissions data and evaluate the subsequent model simulations might be taken as circular reasoning. We note first that observation-derived emissions are frequently used in modelling (for example, Continuous Emissions Monitoring System concentration observations are used to generate emissions data for large stack emitters), and second, that the emissions are only one component of the overall modelling system. An improvement in the simulated VOC concentrations using observation-based emissions is only guaranteed if the emissions dominate the net model error. While our results show that, in general, the new emissions information does improve model performance, the results using that new data are not perfect, indicating other sources of error are contributing to the overall model performance.

3.4 Organic Aerosol (OA) Evaluation

Figure 5 illustrates the histograms for the organic aerosol observations and model results with base case and revised emissions. A clear improvement is shown in the highest concentration bins (>15 $\mu g/m^3$) with the revised emissions. This can be quantified with the 99^{th} percentile of the data (obs=13.4 $\mu g/m^3$, revised=9.3 $\mu g/m^3$, base=4.9 $\mu g/m^3$). The median statistic also improved (obs=2.8 $\mu g/m^3$, revised=0.84 $\mu g/m^3$, base=0.70 $\mu g/m^3$). The lower 5^{th} percentile is also significantly under-predicted compared to observations and does not change much between the two model runs (obs=0.49 $\mu g/m^3$, revised=0.036 $\mu g/m^3$, base=0.035 $\mu g/m^3$). This reflects an under-prediction in the background OA predicted by the model, which is likely due to low

biogenic SOA formation and aging in both model versions. The importance of widespread biogenic SOA formation from boreal forests has been reported in other work (Slowik *et al*., 2010; Tunved *et al*., 2006).

Additional statistics are presented in Table 3. The mean bias, RMSE and slope all improve for the revised-emissions run, though the correlation coefficient decreases significantly for this run. To investigate the variability in the OA bias, we plotted the OA bias as a function of different measured variables. Figure 6 is a plot of the OA bias as a function of the observed black carbon (BC) aerosol for the base-case and sensitivity runs. The BC is a marker for petrochemical combustion, particularly diesel. For the base-case run, the OA negative bias is observed to increase in magnitude with observed BC. Points with high observed BC correlate well with emissions from the OS open-pit mines (Liggio *et al*., 2017), where the BC is likely emitted from the heavy-hauler trucks. The locations with the largest OA bias were also consistent with the locations of mines and the transport wind direction. A review of the OS emission inventories suggest that about 70% of the BC comes from the OS off-road diesel fleet. Including all points, the mean bias improves from -2.8 to -2.4 (see Table 3) when using the revised emissions. Figure 6b shows a zoomed plot for points with high observed BC (>0.8 $\mu g/m^3$). There is a clear improvement in bias for most of these points. The average bias for these high BC points improves from -6.8 $\mu g/m^3$ for the base case to -2.6 $\mu g/m^3$ for the revised emissions. For emissions processing the increase in PM emissions was assigned to the processing plants (particle bin D<1µm) or the surface mines (particle bin D>1µm). Overall, Figure 6 shows that, while the negative OA bias improves for samples high in BC concentration (i.e. influenced by petrochemical combustion or collocated with petrochemical combustion sources), there still remains an unaccounted for negative OA bias. .

Figure 7 is a scatterplot of the difference in predicted POA between the revised and base-case emissions runs vs. the difference in predicted total OA. A large fraction of the points fall along the 1:1 line, and hence for these points the difference between the two runs is almost completely due to the increased total primary PM emissions, and increased POA fraction of those emissions, of the revised emissions simulations. The points with largest concentrations along the 1:1 line correspond to flights over the Syncrude Mildred Lake facility on Aug. 16, Aug. 23 and Sept. 3. There is a subset of points, however, that lies below the 1:1 line; these correspond to points with significantly enhanced model SOA between the two runs (Aug. 16 flight over CNRL Horizon and Aug. 21 survey flight over Shell Muskeg/Jackpine). The SI section includes the model and measurement time series comparisons for the flights on August 21, August 23 and September 3. Overall, the case studies showed improved predictions for the magnitude of the organic aerosol change for the plume passages with the revised emissions; however, the base line organic aerosol was over-predicted for all case studies.

3.4.2 Organic Aerosol Model Recommendations

The improvement in model PM_1 OA bias due to the use of the revised emissions is encouraging; however, the decrease in correlation coefficient suggests that the spatial allocation of PM_1 emissions may need further refinement. The remaining negative bias suggests that other important processes may be missing or under-represented in the model. Three recommendations emerge from recent and current work:

1) SOA Formation from Fugitive IVOC Emissions

Recent publications suggest that fugitive intermediate volatile organic (IVOC) emissions from the OS open-pit mines are needed to represent SOA formation downwind of the OS region (Liggio *et al.*, 2016). In our emissions revision, only a small portion of the IVOCs (dodecane

C_{12}) were added and lumped into the long-chain ALKA lumped species. IVOC species with carbon number ≥13 were not measured by the Li *et al*., (2017) aircraft study and thus we do not have revised IVOC emissions included in this work. Furthermore, the ALKA lumped species has an SOA yield more representative of a lower molecular-weight range, and the yield is known to increase with increasing carbon number, so the dodecane SOA contribution would be underestimated. Work is currently underway with GEM-MACH to implement a Volatility Basis Set (VBS) approach to SOA formation. The VBS approach will more adequately represent the intermediate and semi-volatile volatility range and chemical aging of this lower volatility compounds (Robinson *et al*., 2006). Future work will measure IVOC emissions using box flights around the oil sand facilities and open-pit mines. This will remove current uncertainties in models and help improve the negative bias in plumes. Implementing the VBS scheme will also enable the PM emissions used here (in both data sets) to be distributed into volatility bins.

Also, while the measurement-derived emissions are missing the IVOCs, the measurement-derived POA emissions may contain some gaseous VOCs, IVOCs and SVOC species that react quickly and in one oxidation step yield products that condense onto particles. This rapid SOA mass produced would be measured in the box flights and, at least partially, accounted for in the updated OA emissions; however labeled here as POA instead of fresh SOA. Furthermore, there is the potential for double counting if some of the very reactive gaseous precursors react to form SOA and this is accounted for in the measured POA. In this paper, we have tried to minimize this effect by examining the model performance in the "near field" from emission flights close to facilities. This will be the topic of future box modelling work with the new 2018 measurement-derived IVOC and SVOC emissions to determine how much of the measurement-derived POA is

derived from the fugitive open-pit mining IVOC and SVOC emissions and their rapid particle formation.

2) Background Organic Aerosol Levels

The under-prediction in background OA was a general finding from the study; the cause is believed to be due to underestimated biogenic SOA, due to the lumping of biogenic monoterpene emissions into the anthropogenic ALKE model species in the model's gas-phase mechanism, and the lack of speciated representation of other biogenic SOA precursors such as sesquiterpenes. Future work will update the biogenic SOA yield coefficients in the VBS approach using recent smog chamber results which account for gas-phase loss of organic species to chamber walls (Ma *et al*., 2017).

3) Spatial Allocation of Emissions

Future field studies should also focus on improving within-facility spatial allocation. For example, within-facility data such as the GPS location of the mining trucks would be helpful to derive their activity diurnal profiles and to improve truck emission spatial allocation within a facility. The GPS data would also be useful to define the location of freshly excavated open-pit mines within a facility.

Conclusions

Overall, the weight of evidence suggests that the top-down emission estimation technique applied to the OS surface mining facilities helps to better constrain reported facility-total organic emissions including fugitive sources, as shown by improved model results when the revised emissions are employed. We note that emissions from these sources are a challenge to calculate in bottom-up inventories due to the potential for fugitive emissions. For the mono- and multi-substituted aromatics (TOLU and AROM), the emission rates from facilities were more fine

adjustments, as some facility totals went up and some went down and the overall biases compared to observations improved for AROM but degraded for TOLU. However, the model's ability to predict very high aromatic concentrations in plumes improved with the revised emissions, as shown by the 99th percentile statistic and the case studies.

For the long-chain ALKA species, the revised emissions may have over-corrected, on average, as shown by the increase in mean bias for the entire aircraft data set. However, the correlation coefficient did improve significantly for the long-chain alkane predictions, suggesting the combination of alkane emission increases for some facilities and decreases for others helped to improve the spatial distribution of ALKA emissions. The results for some facilities suggest that further improvement could be achieved by putting more emissions at extraction processing plant locations (i.e., adjusting within-facility spatial allocation). Interestingly, the alkane emission increases and aromatic emission decreases, derived from aircraft data (Li *et al.*, 2018), were associated with the facilities that use paraffinic solvents for bitumen extraction (e.g. Shell Muskeg/Jackpine). Overall, the predictions of alkanes in high concentration plumes improved with the revised emission data set, as shown by the 99th percentile statistic.

For PM_1 organic aerosol, the revised emissions improved the mean bias for predictions; however, a negative bias still exists and the improvement was associated with a decrease in correlation coefficient. The increase in predicted PM_1 OA concentration was largely due to the increase in POA emissions in the revised emissions input files. The POA emissions increased because of a combination of larger measurement-derived PM_1 emissions and the revised ground-observed PM speciation profile having a larger POA fraction. The increase in PM_1 POA emissions were largely allocated spatially to stack locations and this allocation may be a key factor in the degradation of the correlation coefficient, especially if the fine OA originates from

mine-face fugitive emissions. Future work should focus on improving within-facility spatial allocation of emissions. The remaining negative bias in plumes likely stems from missing IVOC emissions in both the emission data sets used here, as suggested by Liggio *et al.* (2015). Ongoing field work to measure the IVOC emissions using aircraft box flights is underway in a new 2018 measurement intensive. Upcoming modelling work with GEM-MACH will include the VBS approach to better represent lower volatility compounds.

Acknowledgements

The authors are grateful to all of the participants in the 2013 JOSM intensive field study for their commitment. The authors are also appreciative of the ECCC Pollutant Inventory and Reporting Division (PIRD) and the U.S. EPA for developing, maintaining, and distributing each country's national emission inventories. We also appreciate the efforts of George Marson of ECCC in helping to compile the various emissions inventories from Alberta Environment and Parks, and also CEMA. We also appreciate the analysis of the NAPS VOC measurement group. This study was funded by the Joint Oil Sands Monitoring program and the Climate Change and Air Quality Program.

References

Akingunola, A., Makar, P.A., Zhang, J., Darlington, A., Li, S.M., Gordon, M., Moran, M.D., and Zheng, Q., Evaluation of GEM-MACH Air Quality Modelling at 2.5km Resolution Using JOSM 2013 Intensive Campaign: Impact of Continuous Monitoring Emissions Stack Parameters on Model Simulations, accepted in ACP, **2018**.

Barsanti, K.C., Carlton, A.G., and Chung, S.H., Analyzing experimental data and model parameters: Implications for predictions of SOA using chemical transport models, Atmos. Chem. and Phys., 13 (23), 12073-12088, **2013**.

Cappa, C.D. and Jimenez, J., Quantitative estimates of the volatility of ambient organic aerosol, Atmos. Chem. Phys., 10 (12), 5409-5424, **2010**.

Cappa, C.D. and Wilson, K.R., Evolution of organic aerosol mass spectra upon heating: Implications for OA phase and partitioning behavior, Atmos. Chem. and Phys., 11 (5), 1895-1911, **2011**.

Chai, T., Kim, H.-C., Lee, P., Tong, D., Pan, L., Tang, Y., Huang, J., McQueen, J., Tsidulko, M., and Stajner, I., Evaluation of the United States National Air Quality Forecast Capability experimental real-time predictions in 2010 using Air Quality System ozone and NO2 measurements, Geoscientific Model Development, 6 (5), 1831-1850, **2013**.

Cho, S., McEachern, P., Morris, R., Shah, T., Johnson, J., and Nopmongcol, U., Emission sources sensitivity study for ground-level ozone and PM 2.5 due to oil sands development using air quality modeling system: Part I- model evaluation for current year base case simulation, Atmos. Environ., 55, 533-541, **2012**.

Cohan, D.S. and Napelenok, S.L., Air Quality Response Modeling for Decision Support, Atmosphere, *2*, 407-425, **2011**.

Côté, J., Gravel, S., Méthot, A., Patoine, A., Roch, M., and Staniforth, A., The operational CMC/MRB global environmental multiscale (GEM) model. Part 1: design considerations and formulation, Mon. Wea. Rev., 126, 1373-1395, **1998**.

Côté, J., Desmarais, J.-G., Gravel, S., Méthot, A., Patoine, A., Roch, M., and Staniforth, A., The operational CMC-MRB global environment multiscale (GEM) model. Part II: results, Mon. Wea. Rev., 126, 1397-1418, **1998**.

Dann, T.F., Wang, D.K., Ambient air benzene concentrations in Canada (1989-1993): Seasonal and day of week variations, trends, and source influences, Journal of the Air and Waste Management Association, 45 (9), pp. 695-702, **1995**.

Davies, M., Person, R., Nopmongcol, U., Shah T., Vijayaraghavan, K., Morris, R., and Picard, D., Lower Athabasca Region Source and Emission Inventory, report prepared by Stantec Consulting Ltd. and ENVIRON International Corporation for Cumulative Environmental Management Association - Air Working Group, http://library.cemaonline.ca/ckan/dataset/0cfaa447-410a-4339-b51f-e64871390efe/resource/fba8a3b0-72df-45ed-bf12-8ca254fdd5b1/download/larsourceandemissionsinventory.pdf, 274 pp., **2012** (last accessed on October 24, 2017).

Dickson, R.J. and Oliver, W.R., Emissions models for regional air quality studies, Environ. Sci. Technol., 25, 1533-1535, **1991**.

Donahue, N.M., Robinson, A.L., Trump, E.R., Riipinen, I., and Kroll, J.H., Volatility and aging of atmospheric organic aerosol, Topics in Current Chemistry, 339, 97-144, **2014**.

Environment and Climate Change Canada & Alberta Environment and Parks: Joint Oil Sands Monitoring Program Emissions Inventory Compilation Report, http://aep.alberta.ca/air/reports-data/documents/JOSM-EmissionsInventoryReport-Jun2016.pdf, 146 pp, **2016**.

Eyth, A., Mason, R., and Zubrow, A.: Development and Status of EPA's 2011 Modeling Platform, 12th CMAS Conference, 28-30 Oct., Chapel Hill, North Carolina, https://www.cmascenter.org/conference//2013/slides/eyth_development_status_2013.pptx, **2013**.

Gentner, D.R., Jathar, S.H., Gordon, T.D., Bahreini, R., Day, D.A., El Haddad, I., Hayes, P.L., Pieber, S.M., Platt, S.M., De Gouw, J., Goldstein, A.H., Harley, R.A., Jimenez, J.L., Prévôt, A.S.H., and Robinson, A.L., Review of Urban Secondary Organic Aerosol Formation from Gasoline and Diesel Motor Vehicle Emissions, Environ. Sci. Technol., 51 (3), 1074-1093, **2017**.

Girard, C., Plante, A., Desgagné, M., Mctaggart-Cowan, R., Côté, J., Charron, M., Gravel, S., Lee, V., Patoine, A., Qaddouri, A., Roch, M., Spacek, L., Tanguay, M., Vaillancourt, P.A., and Zadra, A., Staggered vertical discretization of the canadian environmental multiscale (GEM) model using a coordinate of the log-hydrostatic-pressure type, Monthly Weather Review, 142, 1183-1196, **2014**.

Gong, S.L., Barrie, L.A., Blanchet, J.-P., von Salzen, K., Lohmann, U., Lesins, G., Spacek, L., Zhang, L.M., Girard, E., Lin, H., Leaitch, R., Leighton, H., Chylek, P., and Huang, P., Canadian Aerosol Module: A size-segregated simulation of atmospheric aerosol processes for climate and air quality models 1. Module development, J. Geophy. Res. Atmos., 108, **2003**.

Gordon, M., Li, S.-M., Staebler, R., Darlington, A., Hayden, K., O'Brien, J., and Wolde, M., Determining air pollutant emission rates based on mass balance using airborne measurement data over the Alberta oil sands operations. Atmos. Meas. Tech., 8, 3745–3765. doi:10.5194/amt-8-3745-2015, **2015**.

Government of Canada, Notice with respect to the substances in the National Pollutant Release Inventory for 2018 and 2019, Canada Gazette Part I, Vol. 152, No. 3, pp. 129-172, ISSN 1494-6076, Ottawa, January 20, **2018**.

Griffin, R.J., Cocker III, D.R., Flagan, R.C., and Seinfeld, J.H., Organic aerosol formation from the oxidation of biogenic hydrocarbons, J. Geophys. Res. Atmos., 104 (D3), 3555-3567, **1999.**

Houyoux, M.R., Vukovich, J.M., Coats, Jr., C.J., Wheeler, N.J.M., and Kasibhatla, P.S., Emission inventory development and processing for the Seasonal Model for Regional Air Quality (SMRAQ) project, J. Geophys. Res., 105, 9079-9090, **2000**.

Jimenez, J.L., Canagaratna, M.R., Donahue, N.M., Prevot, A.S.H., Zhang, Q., Kroll, J.H., DeCarlo, P.F., Allan, J.D., Coe, H., Ng, N.L., Aiken, A.C., Docherty, K.S., Ulbrich, I.M., Grieshop, A.P., Robinson, A.L., Duplissy, J., Smith, J.D., Wilson, K.R., Lanz, V.A., Hueglin, C., Sun, Y.L., Tian, J., Laaksonen, A., Raatikainen, T., Rautiainen, J., Vaattovaara, P., Ehn, M., Kulmala, M., Tomlinson, J.M., Collins, D.R., Cubison, M.J., Dunlea, E.J., Huffman, J.A., Onasch, T.B., Alfarra, M.R., Williams, P.I., Bower, K., Kondo, Y., Schneider, J., Drewnick, F., Borrmann, S., Weimer, S., Demerjian, K., Salcedo, D., Cottrell, L., Griffin, R., Takami, A., Miyoshi, T., Hatakeyama, S., Shimono, A., Sun, J.Y., Zhang, Y.M., Dzepina, K., Kimmel, J.R., Sueper, D., Jayne, J.T., Herndon, S.C., Trimborn, A.M., Williams, L.R., Wood, E.C., Middlebrook, A.M., Kolb, C.E., Baltensperger, U., and Worsnop, D.R., Evolution of organic aerosols in the atmosphere, Science, 326 (5959), 1525-1529, **2009**.

Kanakidou, M., Seinfeld, J.H., Pandis, S.N., Barnes, I., Dentener, F.J., Facchini, M.C., Van Dingenen, R., Ervens, B., Nenes, A., Nielsen, C.J., Swietlicki, E., Putaud, J.P., Balkanski, Y., Fuzzi, S., Horth, J., Moortgat, G.K., Winterhalter, R., Myhre, C.E.L., Tsigaridis, K., Vignati, E., Stephanou, E.G., and Wilson, J., Organic aerosol and global climate modelling: A review, Atmos. Chem. Phys., 5 (4), 1053-1123, **2005**.

Kelly, J., Makar, P.A., and Plummer, D. Projections of mid-century summer air-quality for North America: effects of changes in climate and precursor emissions, Atmos. Chem. Phys., 12, 5367-5390, **2012**.

Kroll, J.H., Ng, N.L., Murphy, S.M., Varutbangkul, V., Flagan, R.C., and Seinfeld, J.H., Chamber studies of secondary organic aerosol growth by reactive uptake of simple carbonyl compounds, J. Geophy. Res. Atmos., 110 (23), 1-10, **2005**.

Kroll, J.H. and Seinfeld, J.H., Chemistry of secondary organic aerosol: Formation and evolution of low-volatility organics in the atmosphere, Atmos. Environ., 42 (16), 3593-3624, **2008**.

Lee, P. and Ngan, F., Coupling of Important Physical Processes in the Planetary Boundary Layer between Meteorological and Chemistry Models for Regional to Continental Scale Air Quality Forecasting: An Overview, Atmosphere, *2*, 464-483, **2011**.

Lelieveld, J., Evans, J.S., Fnais, M., Giannadaki, D., and Pozzer, A., The contribution of outdoor air pollution sources to premature mortality on a global scale, Nature, 525 (7569), 367-371, **2015**.

Li, S.-M., Leithead, A., Moussa, S.G., Liggio, J., Moran, M.D., Wang, D., Hayden, K., Darlington, A., Gordon, M., Staebler, R., Makar, P.A., Stroud, C.A., McLaren, R., Liu, P.S.K., O'Brien, J., Mittermeier, R.L., Zhang, J., Marson, G., Cober, S.G., Wolde, M., and Wentzell, J.J.B., Differences between measured and reported volatile organic compound emissions from oil sands facilities in Alberta, Canada, Proceedings of the National Academy of Sciences of the United States of America, 114 (19), pp. E3756-E3765, **2017**.

Liggio, J., Li, S.-M., and McLaren, R., Reactive uptake of glyoxal by particulate matter, J. Geophy. Res. Atmos., 110 (10), 1-13, **2005**.

Liggio, J., Li, S.-M., Hayden, K., Taha, Y.M., Stroud, C., Darlington, A., Drollette, B.D., Gordon, M., Lee, P., Liu, P., Leithead, A., Moussa, S.G., Wang, D., O'Brien, J., Mittermeier, R.L., Brook, J.R., Lu, G., Staebler, R.M., Han, Y., Tokarek, T.W., Osthoff, H.D., Makar, P.A., Zhang, J., Plata, D.L., and Gentner, D.R., Oil sands operations as a large source of secondary organic aerosols, Nature, 534 (7605), 91-94, **2016**.

Liggio, J., Stroud, C.A., Wentzell, J. *et al*., Quantifying the primary emissions and photochemical formation of isocyanic acid downwind of Oil Sands operations, Environ. Sci. Technol., doi: 10.1021/acs.est.7b04346, **2017**.

Lopez-Hilfiker, F.D., F.D., Mohr, C., D'Ambro, E.L., Lutz, A., Riedel, T.P., Gaston, C.J., Iyer, S., Zhang, Z., Gold, A., Surratt, J.D., Lee, B.H., Kurten, T., Hu, W.W., Jimenez, J., Hallquist, M., and Thornton, J.A., Molecular composition and volatility of organic aerosol in the Southeastern U.S.: Implications for IEPOX Derived SOA, Environ. Sci. Technol., 50 (5), 2200-2209, **2016**.

Ma, P. K., Zhao, Y., Robinson, A. L., Worton, D. R., Goldstein, A. H., Ortega, A. M., Jimenez, J. L., Zotter, P., Prévôt, A. S. H., Szidat, S., and Hayes, P. L.: Evaluating the impact of new observational constraints on P-S/IVOC emissions, multigeneration oxidation, and chamber wall losses on SOA modeling for Los Angeles, CA, Atmos. Chem. Phys., 17, 9237–9259, **2017**.

Makar, P.A., Gong, W., Milbrandt, J., Hogrefe, C., Zhang, Y., Curci, G., Žabkar, R., Im, U., Balzarini, A., Baró, R., Bianconi, R., Cheung, P., Forkel, R., Gravel, S., Hirtl, M., Honzak, L., Hou, A., Jiménez-Guerrero, P., Langer, M., Moran, M.D., Pabla, B., Pérez, J.L., Pirovano, G., San José, R., Tuccella, P., Werhahn, J., Zhang, J., and Galmarini, S., Feedbacks between air pollution and weather, Part 1: Effects on weather, Atmos. Environ., 115, 442-469, **2015a**.

Makar, P.A., Gong, W., Hogrefe, C., Zhang, Y., Curci, G., Žabkar, R., Milbrandt, J., Im, U., Balzarini, A., Baró, R., Bianconi, R., Cheung, P., Forkel, R., Gravel, S., Hirtl, M., Honzak, L., Hou, A., Jiménez-Guerrero, P., Langer, M., Moran, M.D., Pabla, B., Pérez, J.L., Pirovano, G., San José, R., Tuccella, P., Werhahn, J., Zhang, J., and Galmarini, S., Feedbacks between air pollution and weather, part 2: Effects on chemistry, Atmos. Environ., 115, 499-526, **2015b**.

Makar, P.A. *et al*., Estimates of Exceedances of Critical Loads for Acidifying Deposition in Alberta and Saskatchewan, accepted in ACP, **2018.**

Mashayekhi, R., Zhao, S., Saeednooran, S., Hakami, A., Ménard, R., Moran, M. D., and Zhang, J., Emissions Uncertainty Inventory and Modeling Framework: Case Study of Residential Wood Combustion, 15th Annual CMAS Conference, October 24-26, Chapel Hill, NC, https://www.cmascenter.org/conference//2016/slides/mashayekhi_development_emission_2016.pptx, **2016**.

McNeill, V.F., Aqueous organic chemistry in the atmosphere: Sources and chemical processing of organic aerosols, Environ. Sci. Technol., 49 (3), 1237-1244, **2015**.

Moran, M.D., Ménard, S., Pavlovic, R., Anselmo, D., Antonopoulos, S., Makar, P.A., Gong, W., Gravel, S., Stroud, C., Zhang, J., Zheng, Q., Robichaud, A., Landry, H., Beaulieu, P.A., Gilbert, S., Chen, J., and Kallaur, A., Recent Advances in Canada's National Operational AQ Forecasting System, NATO Science for Peace and Security Series C: Environmental Security, 137, 215-220, **2013**.

Office of the Federal Register National Archives and Records Administration, Protection of Environment, Code of Federal Regulations, Title 40, Parts 50 to 51, Special Edition of the Federal Register, U.S. government publishing office, Washington, DC 20402–0001, July 1, **2015**.

Pankow, J.F., An absorption model of the gas/aerosol partitioning involved in the formation of secondary organic aerosol, Atmos. Environ., 28 (2), 189-193, **1994**.

Park, S.H., Gong, S.L., Bouchet, V.S., Gong, W., Makar, P.A., Moran, M.D., Stroud, C.A., and Zhang, J., Effects of black carbon aging on air quality predictions direct radiative forcing estimation, Tellus, Series B: Chemical and Physical Meteorology, 63 (5), 1026-1039, **2011**.

Pouliot, G., Pierce, T., Denier van der Gon, H., Schaap, M., Moran, M., and Nopmongcol, U., Comparing emission inventories and model-ready emission datasets between Europe and North America for the AQMEII project, Atmos. Environ., 53, 4-14, **2012**.

Pouliot, G., Denier van der Gon, H.A.C., Kuenen, J., Zhang, J., Moran, M.D., and Makar, P.A., Analysis of the emission inventories and model-ready emission datasets of Europe and North America for phase 2 of the AQMEII project, Atmos. Environ., 115, 345-360, **2015**.

Robinson, A.L., Donahue, N.M., Shrivastava, M.K., Weitkamp, E.A., Sage, A.M., Grieshop, A.P., Lane, T.E., Pierce, J.R., and Pandis, S.N., Rethinking organic aerosols: Semivolatile emissions and photochemical aging, Science, 315 (5816), 1259-1262, **2007**.

Rouleau, M., Egyed, M., Taylor, B., Chen, J., Samaali, M., Davignon, D., and Morneau, G., Human health impacts of biodiesel use in on-road heavy duty diesel vehicles in Canada, Environ. Sci. Technol., 47 (22), 13113-13121, 2013.

Schultz, M.G., Diehl, T., Brasseur, G.P., and Zittel, W., Air Pollution and Climate-Forcing Impacts of a Global Hydrogen Economy, Science, 302 (5645), 624-627, **2003**.

Seinfeld, J. H. and Pandis, S. N., Atmospheric Chemistry and Physics from air pollution to climate change, New York. John Wiley and Sons, Incorporated, **1998**.

Shrivastava, M., Easter, R.C., Liu, X., Zelenyuk, A., Singh, B., Zhang, K., Ma, P.-L., Chand, D., Ghan, S., Jimenez, J.L., Zhang, Q., Fast, J., Rasch, P.J., and Tiitta, P., Global transformation and fate of SOA: Implications of low-volatility SOA and gas-phase fragmentation reactions, J. Geophys. Res., 120 (9), 4169-4195, **2015**.

Slowik, J.G., Stroud, C., Bottenheim, J.W., Brickell, P.C., Chang, R.Y.-W., Liggio, J., Makar, P.A., Martin, R.V., Moran, M.D., Shantz, N.C., Sjostedt, S.J., Van Donkelaar, A., Vlasenko, A., Wiebe, H.A., Xia, A.G., Zhang, J., Leaitch, W.R., and Abbatt, J.P.D., Characterization of a large biogenic secondary organic aerosol event from eastern Canadian forests, Atmos. Chem. Phys., 10 (6), 2825-2845, **2010**.

Solazzo, E., Bianconi, R., Pirovano, G., Matthias, V., Vautard, R., Moran, M.D., Wyat Appel, K., Bessagnet, B., Brandt, J., Christensen, J.H., Chemel, C., Coll, I., Ferreira, J., Forkel, R., Francis, X.V., Grell, G., Grossi, P., Hansen, A.B., Miranda, A.I., Nopmongcol, U., Prank, M., Sartelet, K.N., Schaap, M., Silver, J.D., Sokhi, R.S., Vira, J., Werhahn, J., Wolke, R., Yarwood, G., Zhang, J., Rao, S.T., and Galmarini, S., Operational model evaluation for particulate matter in Europe and North America in the context of AQMEII, Atmos. Environ., 53, 75-92, **2012**.

Stroud, C. A., Morneau, G., Makar, P. A., Moran, M. D., Gong, W., Pabla, B., Zhang, J., Bouchet, V. S., Fox, D., Venkatesh, S., Wang, D., and Dann, T., OH-reactivity of volatile organic compounds at urban and rural sites across Canada: Evaluation of air quality model predictions using speciated VOC measurements, Atmos. Environ., 42, 7746-7756, **2008**.

Stroud, C.A., Makar, P.A., Moran, M.D., Gong, W., Gong, S., Zhang, J., Hayden, K., Mihele, C., Brook, J.R., Abbatt, J.P.D., and Slowik, J.G., Impact of model grid spacing on regional- and urban- scale air quality predictions of organic aerosol, Atmos. Chem. Phys., 11 (7), 3107-3118, **2011**.

Stroud, C.A., Zaganescu, C., Chen, J., McLinden, C.A., Zhang, J., and Wang, D., Toxic volatile organic air pollutants across Canada: multi-year concentration trends, regional air quality modelling and source apportionment, J. Atmos. Chem., 73 (2), 137-164, **2016**.

Tunved, P., Hansson, H.-C., Kerminen, V.-M., Ström, J., Maso, M.D., Lihavainen, H., Viisanen, Y., Aalto, P. P., Komppula, M., and Kulmala, M., High natural aerosol loading over boreal forests, Science, 312, 261–263, doi:10.1126/science.1123052, **2006**.

Wang, X., Chow, J. C., Kohl, S. D., Percy, K. E., Legge, A. H., and Watson, J. G., Characterization of PM2.5 and PM10 fugitive dust source profiles in the Athabasca Oil Sands Region, Journal of the Air & Waste Management Association, 65:12, 1421-1433, DOI: 10.1080/10962247.2015.1100693, **2015**.

Zhang, J., Zheng, Q., Moran, M. D., Makar, P. A., Akingunola, A., Li, S.-M., Marson, G., Gordon, M., Melick, R., and Cho, S., Emissions preparation for high-resolution air quality modelling over the Athabasca oil sands region of Alberta, Canada, 21st Intern. Emissions Inventory Conference, 13-17 April, San Diego, http://www.epa.gov/ttn/chief/conference/ei21/session1/zhang_emissions.pdf, 18 pp, **2015**.

Zhang, J. *et al*., Emissions preparation and analysis for Multiscale Air Quality Modelling over the Athabasca Oil Sands Region of Alberta, Canada, accepted in ACP, **2018**.

Table 1. Facility total emission rates for three lumped organic species and $PM_{2.5}$ calculated with the bottom-up, base case inventory, CEMA facility-specific VOC profiles (labeled Base Case) and the top-down measurement-derived rates (labeled Revised Emission case, scaled to tonnes/year for VOCs or tonnes/Aug&Sept for $PM_{2.5}$). Emission rate increase/decrease of more than ±500 tonnes compared to base case is shown in red/blue.

	Suncor – M/S		Syncrude - ML		Shell – MR/J		CNRL - Horizon	
Species	**Base Case**	**Revised**	**Base Case**	**Revised**	**Base Case**	**Revised**	**Base Case**	**Revised**
Mono-Substituted Aromatics (TOLU)	486	1112	806	1539	6.8	72	135	393
Multi-Substituted Aromatics (AROM)	1457	1569	5273	1696	746	88	1125	500
Long Chain Alkanes (ALKA)	5636	13488	12348	10022	1690	14384	2651	23779
Particulate Matter ($PM_{2.5}$)	1251	2537*	1021	3648*	459	2423*	402	1015*

VOC revised-emissions are based on annual estimates, derived in Li *et al.,* (2017). The estimates consider monthly and annual oil production yields reported by facilities for the plant stack emissions. For tailing ponds and mine faces, the VOC estimates are calculated using a surface-to-atmosphere mass transfer model considering ambient temperature and wind speed.

* $PM_{2.5}$ revised emissions are based on 2-month emission (Aug&Sept) rather than based on an annual estimate (Zhang *et al.,* 2018) due to uncertainties in calculating dust emissions in the winter months.

Table 2. Facility-specific VOC speciation profiles (mass fractions) applied to the surface mining facilities in the Athabasca oil sands region compared to standard speciation profiles for Canadian and U.S. petrochemical oil refineries (in ADOM-II chemical speciation). Data are based on Zhang *et al.* (2018) and references therein. All four profiles are used in the base case simulation.

Species	Shell M/J, Syncrude AN, Imperial Kearl Base Case Plant Profile (CEMA)	Syncrude ML, Suncor, CNRL Base Case Plant Profile (CEMA)	CEPS Database Standard Profile #9012 For Oil Refineries in Base Case	SPECIATE Database Standard Profile #0316 For Oil Refineries in Base Case
EC38 (Propane, Benzene, Acetylene)	0.0	0.0	0.247	0.176
EA3 (Alkane ≥C4)	0.90	0.71	0.623	0.781
EA2 (Alkene ≥C3)	0.007	0.069	0.031	0.002
ETOL (Toluene and other mono-aromatics)	0.001	0.057	0.005	0.008
EARO (Multi-functional aromatics)	0.0003	0.099	0.003	0.003
EHCO (Formaldehyde)	0.00001	0.0003	0.110	0.0

Columns do not add up to unity due to "unaccounted for" or "unassigned species" and/or due to consideration of reactivity weighting for the ADOM-II mechanism.

Refinery Profile #9012 is a profile from the Canadian Emissions Processing System (Moran, M.D., M.T. Scholtz, C.F. Slama, A. Dorkalam, A. Taylor, N.S. Ting, D. Davies, P.A. Makar, S. Venkatesh, An Overview of CEPS1.0: Version 1.0 of the Canadian Emissions Processing System for Regional-Scale Air Quality Models. In Proc. 7th AWMA Emission Inventory Symp., Research Triangle Park, North Carolina, Air & Waste Management Association, Pittsburgh, Oct. 28-30, 1997.)

Table 3. Statistical scores from the model simulations with revised and base case emissions; all statistics are relative to observations.

Lumped Species	Simulation	Mean Bias (ppbv)	RMSE (ppbv)	Slope	Y-intercept (ppbv)	Correlation Coefficient, R
TOLU	Base Case	**-0.041**	**0.277**	0.217	**0.063**	**0.32**
	Revised Emissions	0.049	0.386	**0.426**	0.125	0.31
AROM	Base Case	0.152	0.435	**0.957**	0.154	**0.41**
	Revised Emissions	**0.044**	**0.227**	0.383	**0.083**	0.37
ALKA	Base Case	**-0.123**	**5.556**	**0.378**	**2.028**	0.24
	Revised Emissions	1.98	6.403	0.335	4.097	**0.34**
OA	Base Case	-2.79	3.866	0.186	**0.252**	**0.59**
	Revised Emissions	**-2.37**	**3.632**	**0.292**	0.273	0.49

RMSE is the root mean square error. Y-intercept corresponds to the model intercept of a model vs observation correlation plot. Mean bias is the model-observation mean score. The better score for a given pair of statistics is shown in **bold-face** font.

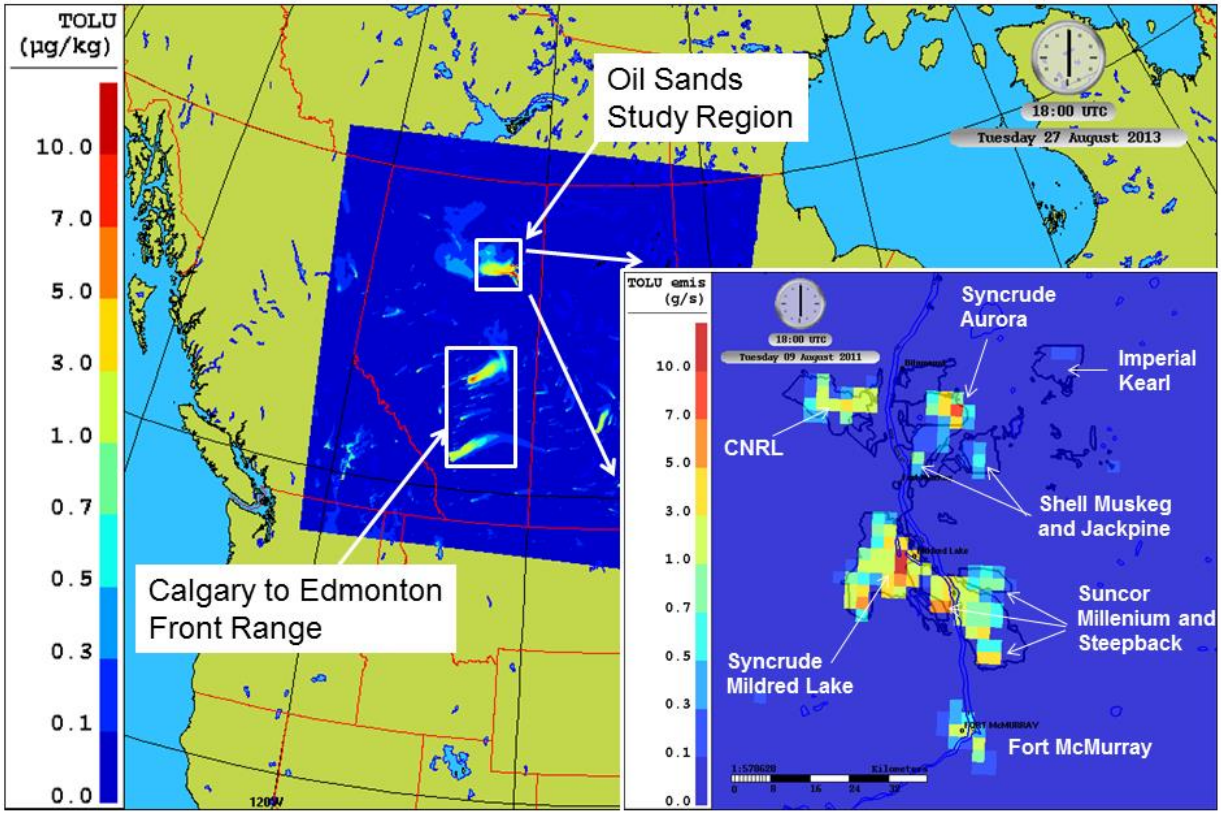

Figure 1. The background image is the nested domain, at 2.5-km grid spacing, covering all of Alberta and Saskatchewan and encompassing the Athabasca Oil Sand study region (white box). The model field shown is for the lumped toluene species (TOLU) mass mixing ratio (µg/kg air). The inserted image on the right is the TOLU emission map (g/s/grid cell) for the Oil Sands study region at the same hour as mixing ratio image on the left. The Oil Sand facility's names are listed in white labels.

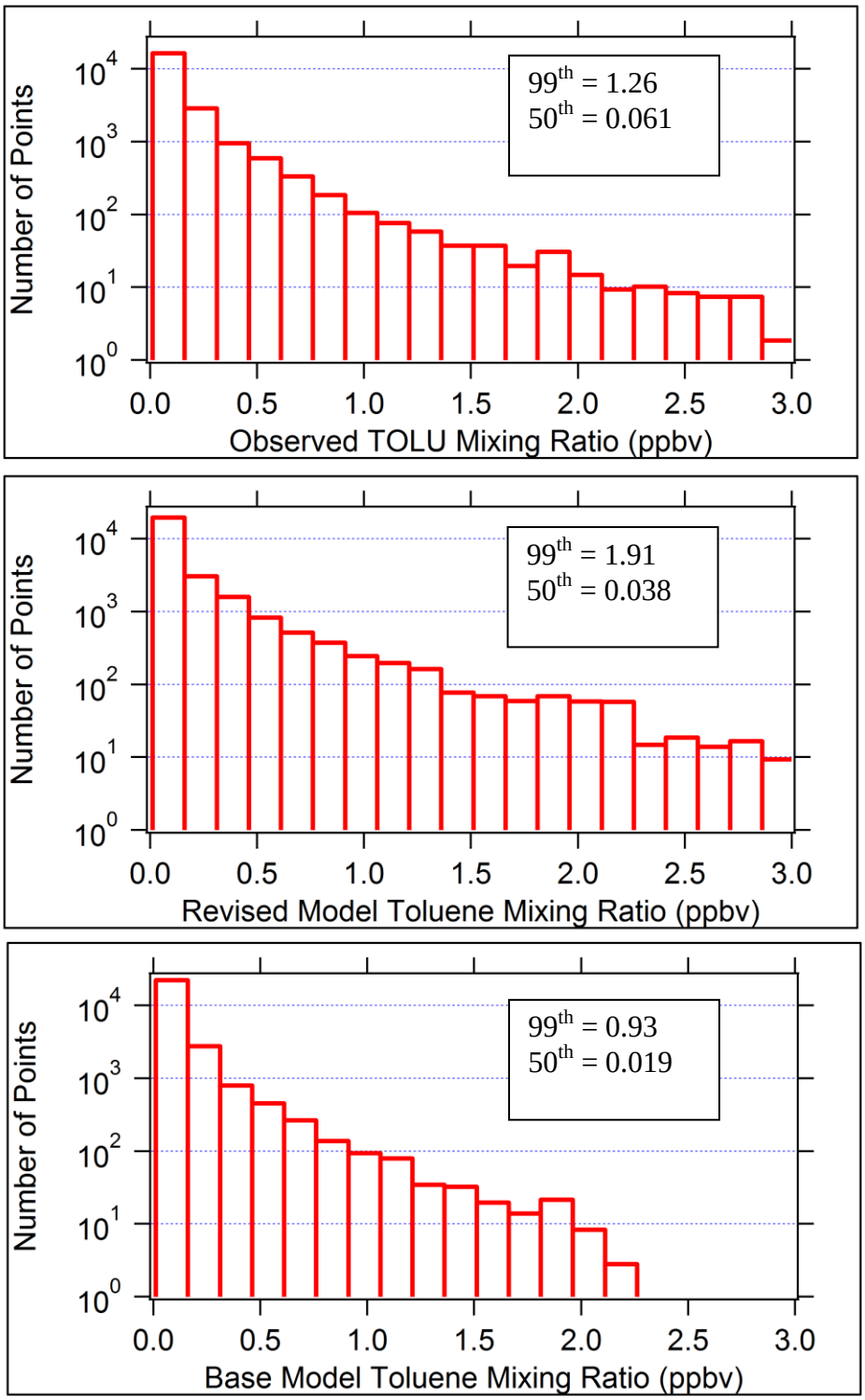

Figure 2. Histograms for (a) observed TOLU, (b) revised-emissions TOLU, and (c) base-case-emissions TOLU volume mixing ratios (ppbv). Points correspond to 10-sec averaged aircraft and model data, sorted into 20 bins by volume mixing ratio. The inset boxes show the 50th and 99th percentile values for each histogram.

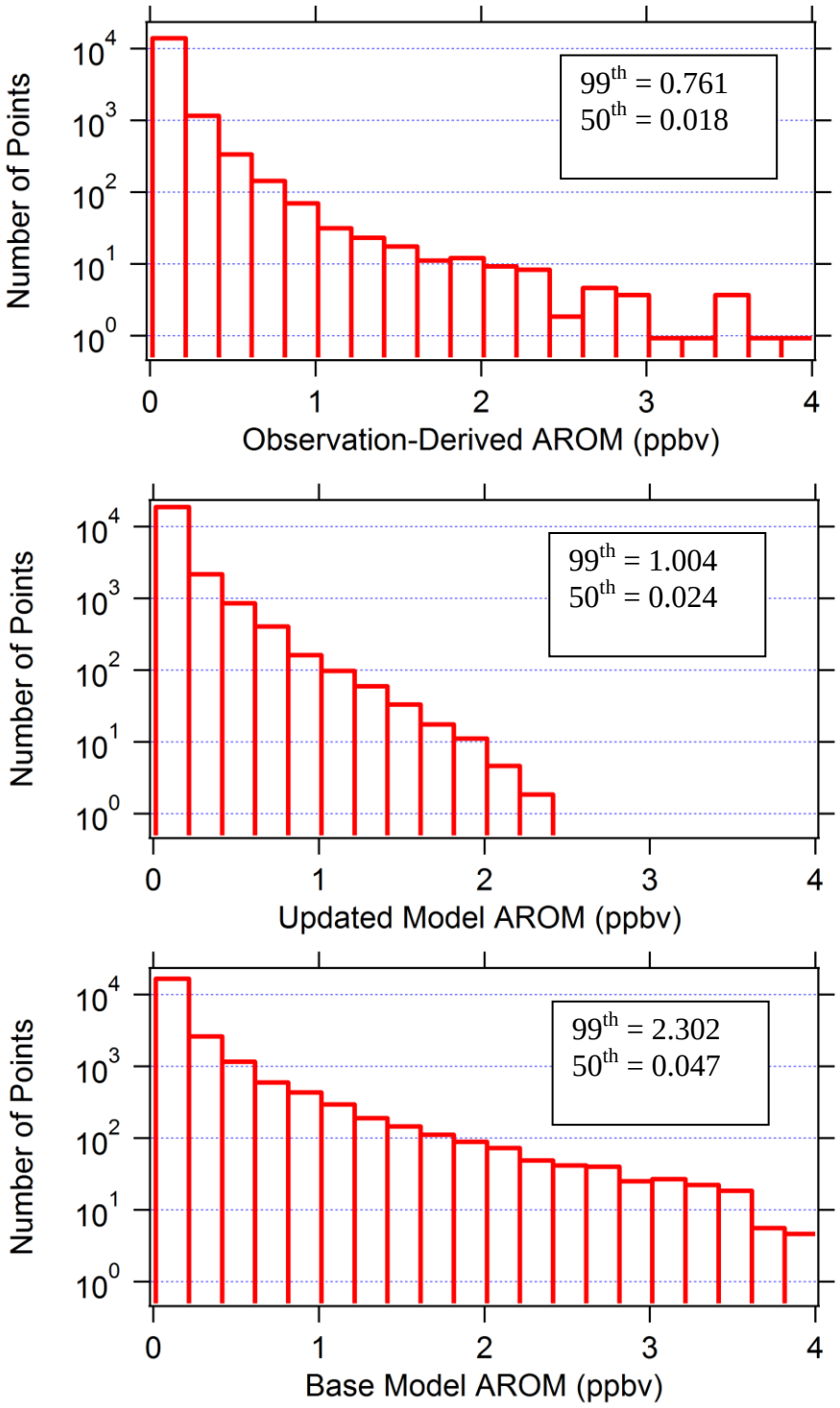

914

915 Figure 3. Histograms for (a) observed AROM, (b) revised-emissions AROM, and (c) base model AROM
916 volume mixing ratios (ppbv). Points correspond to 10-sec averaged aircraft and model data, sorted into
917 20 bins by volume mixing ratio. The inset boxes show the 50th and 99th percentile values for each
918 histogram

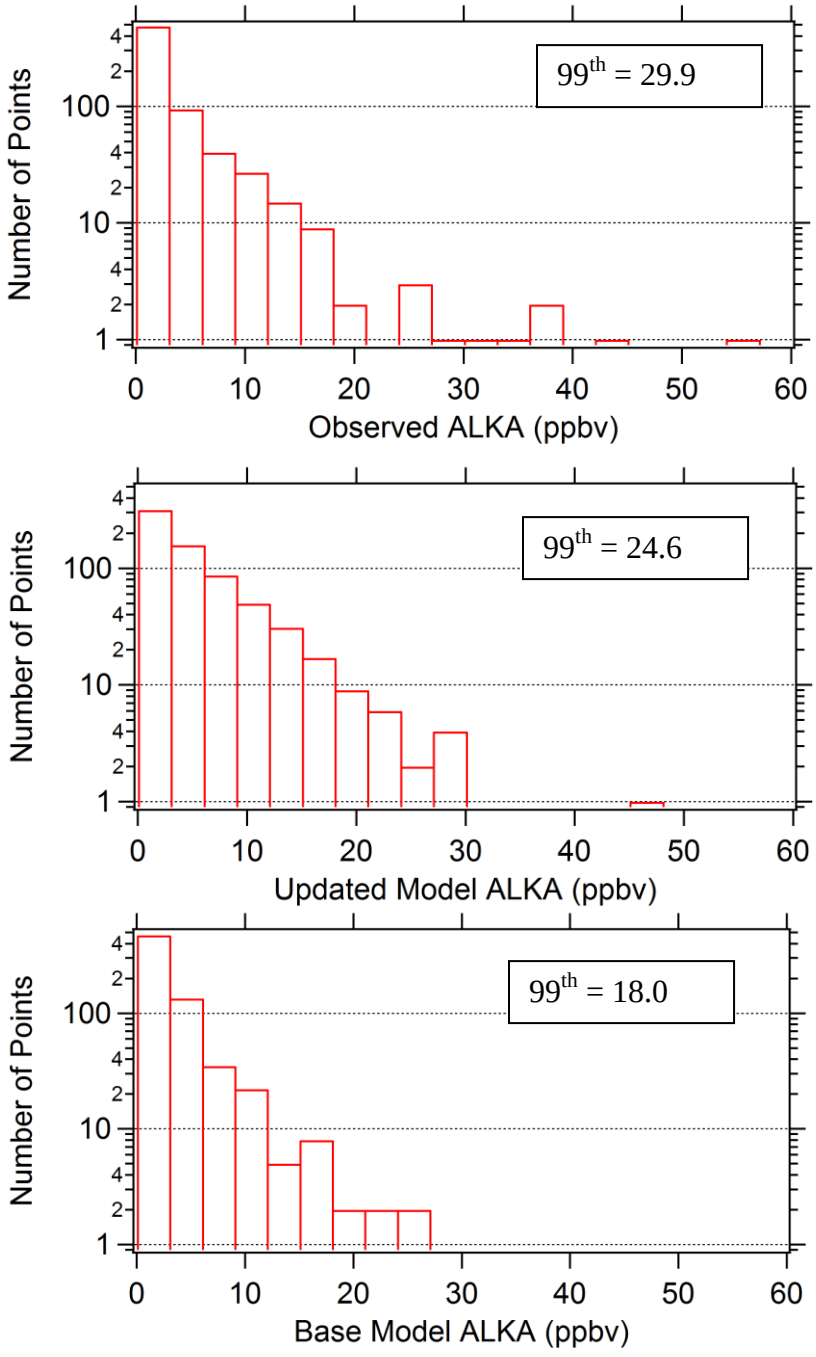

Figure 4. Histograms for (a) observed ALKA, (b) revised-emissions ALKA, and (c) base-case emissions ALKA volume mixing ratios (ppbv). Points correspond to canister grab samples and model data, sorted into 20 bins by mixing ratio. The inset boxes show the 99th percentile value for each histogram.

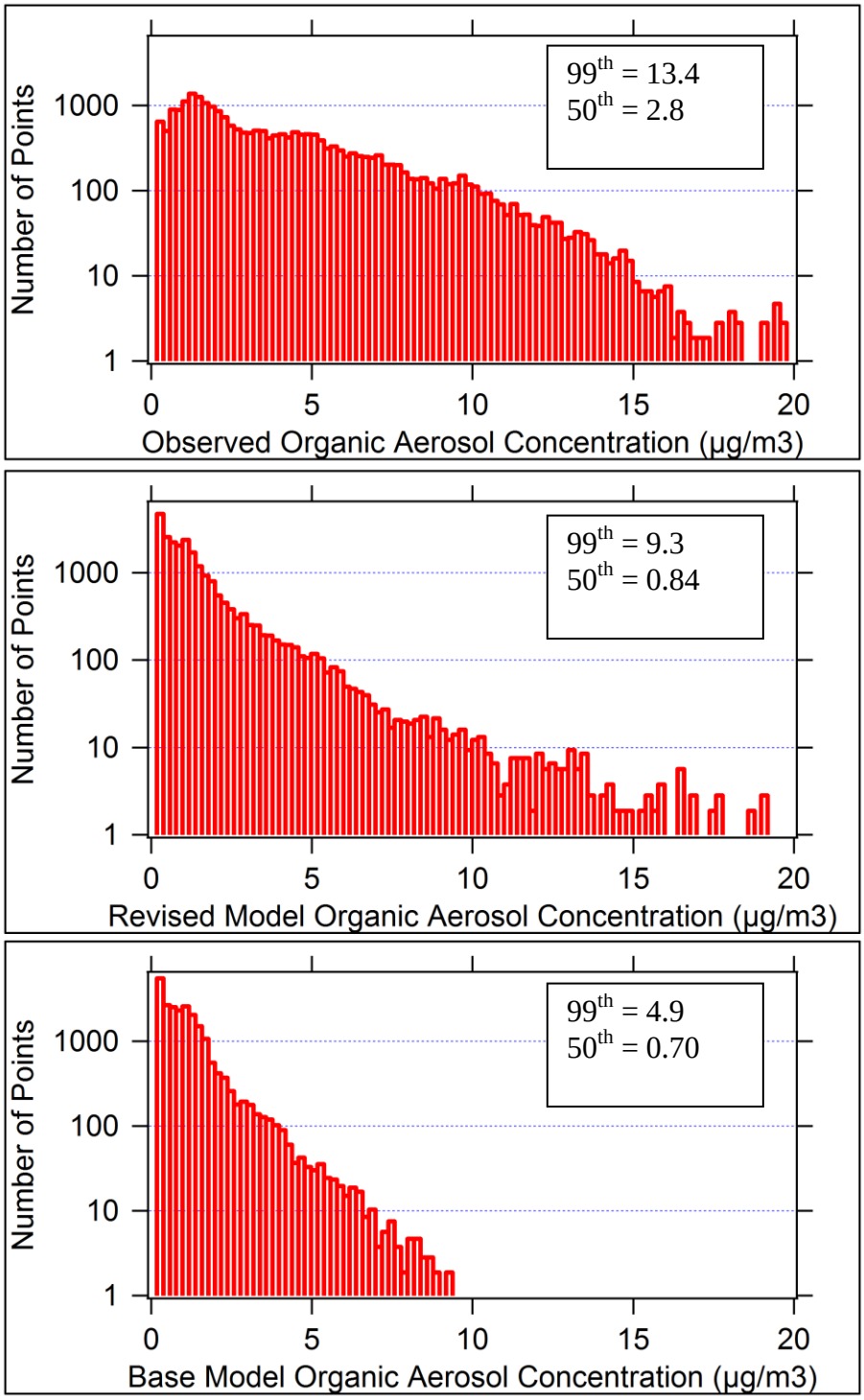

946

947 Figure 5. Histograms for (a) observed organic aerosol (OA), (b) revised-emissions OA, and (c) base-
948 case emissions OA concentrations (µg/m^3). Points correspond to 10-sec averaged aircraft and model
949 data. The inset boxes show the 50th and 99th percentile values for each histogram.

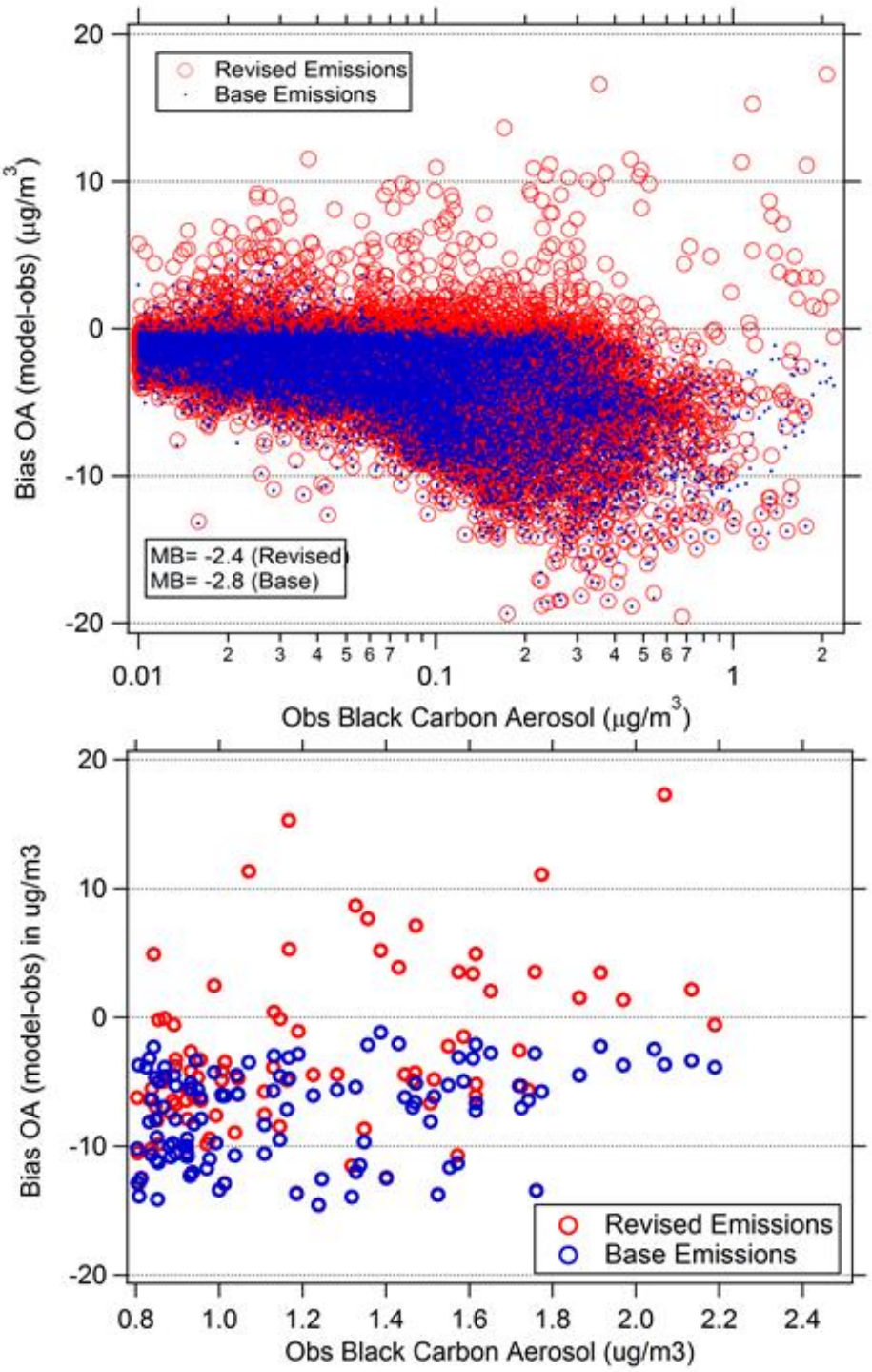

950

951 Figure 6ab. Organic aerosol model bias as a function of observed black carbon aerosol. The
952 bottom panel is an enlargement of the upper panel showing only the data points for observed
953 BC>0.8 µg/m^3. The model results for the base-case emissions run are plotted in blue and points
954 in red correspond to the revised-emissions run. The data plotted is for all the aircraft flights.

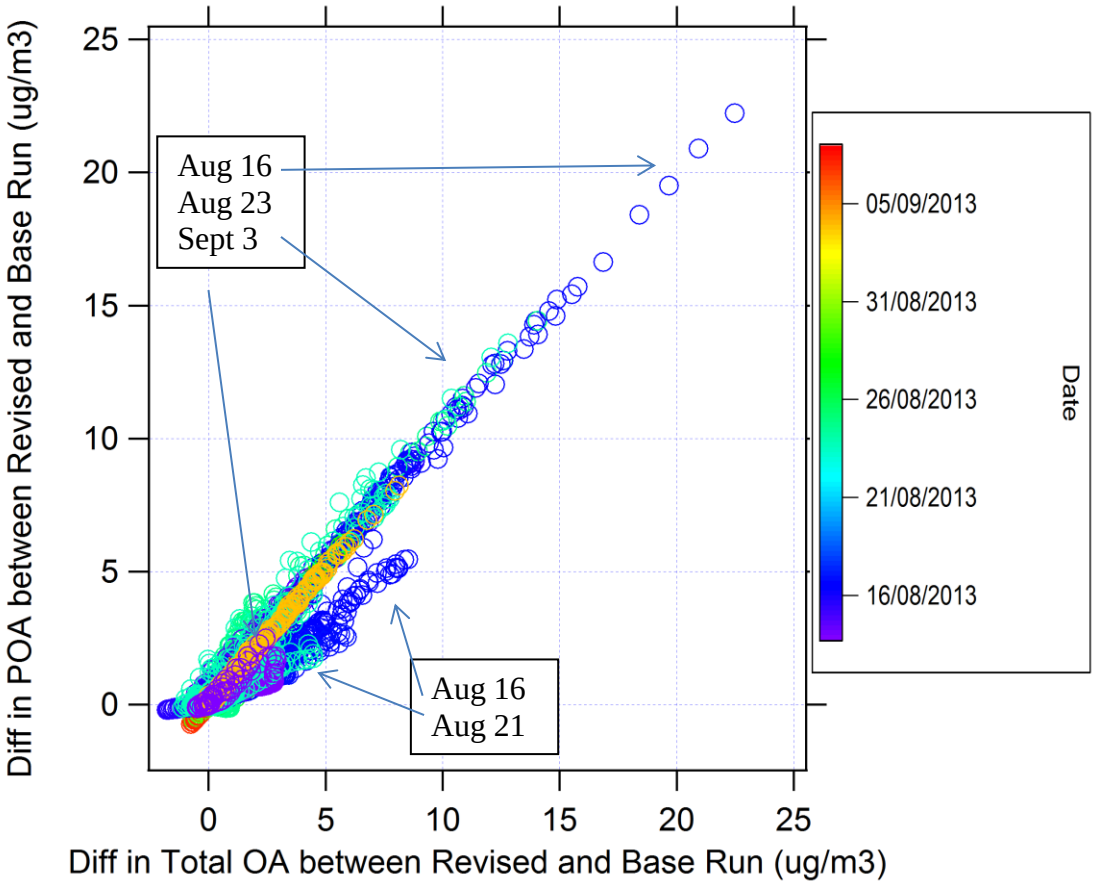

Figure 7. Difference in predicted POA concentrations between revised-emissions and base-case runs plotted as a function of the difference in predicted total OA concentration between the revised-emissions and base-case runs for all flights. Points along the 1:1 line show a difference solely from POA emission changes. Points below the 1:1 line show enhanced SOA formation.